Mem. Fac. Eng., Kyoto Univ. Vol. 52, No. 1 (1990)

Evaluation of Solid Electrode Array Effects in Computerized Section Construction Procedure for Resistivity Interpretation

by

Tsuyoshi SUGANO*

(Received September 27, 1989)

Abstract

The future effectiveness of the resistivity method depends upon its ability to interpret field data obtained under more complex geological structure environments, such as weathered overburden layers, vertical contacts, faults, fracturezones, deep bed rocks or host rocks, nearsurface lateral or local inhomogeneities and various topographies.

Electrical solid array resistivity techniques by using hole-to-surface and cross-hole electrode configurations may be able to extract and enhance the responses (signals) due to deep or small target inhomogeneities. Recently, in geophysical prospecting, some tomographic reconstruction algorithms have been investigated. Especially, the tomographic analysis of seismic data has lately become a powerful tool for geophysical researches. In this study, the electrical solid array effects for the computerized section construction procedure have been evaluated. Investigating the solid array element effects in the initial procedure of the tomographic image reconstruction from resistivity measurements has important interpretive advantages.

In this paper, some following points are discussed;

(1) Sensitivity distribution technique as an aid to investigate the characteristics of the tomography solid electrode arrays.
(2) Significance of electrode-probing configuration and array combination pattern design.
(3) Resistivity computerized section construction procedure by using the sensitivity distribution technique to the inverse problem.
(4) An evaluation of solid electrode array effects in the resistivity computerized section construction procedure.

1. Introduction

Recently, new electrical prospecting techniques utilizing the three-dimensional data and the subsurface electrodes have become very important exploration

* Department of Mineral Science and Technology

tools for detecting deeply located mineral or low mineralized deposits, energy and groundwater reservoirs and geological fracture zones.[1),7-12),27-30),43-44),48-49] The most important recent developments in electrical methods include the refinement of modeling techniques and the uses of high density numerical modelings and the three-dimensional subsurface solid electrode array configurations.[4-13),22),25-30),38-45),48-49] The electrical solid array resistivity techniques by using the hole-to-surface and cross-hole electrode configurations are very useful for the extraction and enhancement of the responses due to deeper or smaller target inhomogeneities under complicated resistivity environments.

Generally, in the traditional resistivity prospecting techniques, surface electrode array configurations have been mainly used. Recently, in geophysical prospecting, some tomographic reconstruction algorithms have been developed. Especially, the tomographic analysis of seismic data has lately become a very powerful tool for geophysical researches.[32)] On the other hand, in the electrical prospecting method, the fundamental studies on the computerized tomography technique by using the hole-to-surface and cross-hole solid arrays have been tried by Daily and Yorkey (1988)[41)] at the Lawrence Livermore National Laboratory and by Beasley and Ward[42)] at the University of Utah. Basically, Tripp et al., (1984)[33)] already used the tomography procedure as an inversion of the surface electrical array data. Some approaches to tomography procedure for the electrical data have lately been investigated. However, a sufficient technique to be applied has not been established. Also, the usefulness of electrical tomographic image reconstruction from solid array resistivity measurements has not been evaluated sufficiently.

The present study suggests that the investigation of the electrical solid array effects in the computerized tomography procedure provide many interpretive advantages. It is worth special mention that evaluating the effects of electrical solid arrays and designing the effective electrode combination pattern are found to be sensitive to the computerized section constructions. This paper begins with a brief review of the sensitivity distributions for solid electrode arrays as the tomography elements in Section 2. They have been calculated by the forward problem modelings, such as the analytical, the finite element or the finite difference two and three-dimensional (2D-3D) and three-dimensional (3D) algorithms. Next, Section 3 presents the construction procedure of the resistivity computerized section using the sensitivity distribution technique to the inverse problem. Section 4 discusses three kinds of evaluations for the solid array effects in the resistivity computerized section construction process. The first evaluation of the solid array effects in the computerized section construc-

tion has been studied about the electrode array geometric configuration effects. The second evaluation has been investigated about the electrode array spacing and line effects. The third evaluation has been performed about the electrode array combination effects. In this study, four kinds of solid arrays have been chosen to investigate the range of applications to the practical problems. Consequently, Section 5 gives conclusions.

2. Sensitivity distributions of solid electrode array elements for electrical tomography procedure

The most important recent developments are the uses of numerical modeling techniques such as the finite element or the finite difference two and three-dimensional (2 D-3 D) and the three-dimensional (3 D) solutions, and the resistivity measurements using hole-to-surface and cross-hole solid electrode arrays driven in boreholes or tunnels. The solid array system can extract and enhance the responses due to deep, ill rich and small target inhomogeneities with higher sensitivity than the surface array system. Also, the solid array system using subsurface electrodes has various electrode-probing configurations, and array combination patterns.

Some solid arrays overcome most of the surface arrays in their sensitivity characteristics.

Figures 1 a and 1 b show arbitrary solid electrode array configurations and target inhomogeneities in the cases of infinite space and half-space. The apparent resistivity acquired by the solid electrode array in the case of the infinite space shown in Figure 1 a is given by the following equation:

$$\rho_a = G(V/I)$$
$$G = 4\pi(1/C_1P_1 + 1/C_2P_2 - 1/C_1P_2 - 1/C_2P_1)^{-1}, \quad (1)$$

where G is the so-called geometric configuration factor. V is the potential difference between P_1 and P_2, and I is the current between C_1 and C_2. The geometric factor converts the measured ohmic factor (V/I) for any arbitrary solid electrode array configuration to resistivity of the medium. In the case of half-space shown in Figure 1 b, the apparent resistivity is given by the following equation in consideration of the electrical images by an air-earth interface,

$$\rho_a = G(V/I)$$
$$G = 4\pi(1/C_1P_1 + 1/C_2P_2 - 1/C_1P_2 - 1/C_2P_1 + 1/C_1'P_1 + 1/C_2'P_2 - 1/C_1'P_2 - 1/C_2'P_1)^{-1}. \quad (2)$$

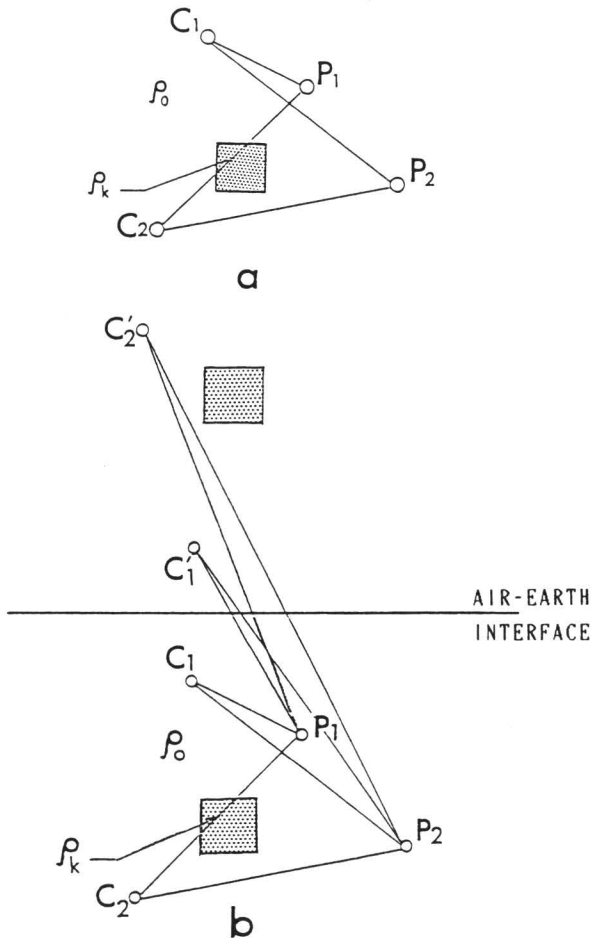

Fig. 1. Arbitrary solid electrode array and target inhomogeneity.
(a) : Infinite space, (b) : Half-space.

For the usual case where the infinite space and half-space are not composed of uniform resistivity materials, the values derived using Equations (1) and (2) are termed the apparent resistivities.

Figure 2 shows the resistivity computer model which has a background resistivity ρ_N (in this homogeneous case, $\rho_N=\rho_0$) of 100 ohm-m, and the darker region corresponded to a resistivity ρ_k of 10 ohm-m, a ratio of 1 : 10. In the forward problem by giving the resistivity contrast, the current source and the potential electrode positions, one can obtain a sensitivity distribution using the

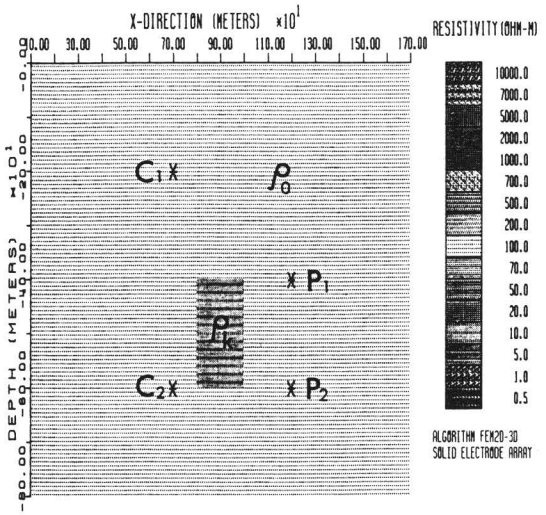

Fig. 2. A computer model of cross-hole electrode array and target inhomogeneity of which resistivity $\rho_k = 10$ ohm-m in the medium of $\rho_0 = 100$ ohm-m.

numerical technique, such as the FEM 2 D– 3 D and the network 3 D algorithms, approximating the solution to the following Laplace equation:

$$\begin{aligned} \nabla \cdot (1/\rho \nabla V) &= 0 \quad \text{in the domain of interest,} \\ (1/\rho)\, \partial V/\partial n &= j \quad \text{on its boundary,} \end{aligned} \tag{3}$$

where $\rho(x, y, z)$ is the resistivity distribution, which is everywhere real and positive, $V(x, y, z)$ the potential distribution, n the outward normal, j the electric current density.

In the FEM 2 D– 3 D modeling algorithm, the λ–domain potential $V\lambda(x, \lambda, z)$ is tranformed into the three–dimensional potential $V(x, y, z)$ by the Fourier inverse transform,

$$V(x, y, z) = \frac{1}{2\pi} \int_{-\infty}^{\infty} V_\lambda(x, \lambda, z)\ e^{i\lambda y}\, d\lambda. \tag{4}$$

The sensitivity distribution can be obtained as a next expression.[1–6), 14–16), 20), 48–49)]

Define:

1) ρ_{ak}, the apparent resistivity (ohm–m) of the inhomogeneous earth with target inhomogeneities computed by the FEM.

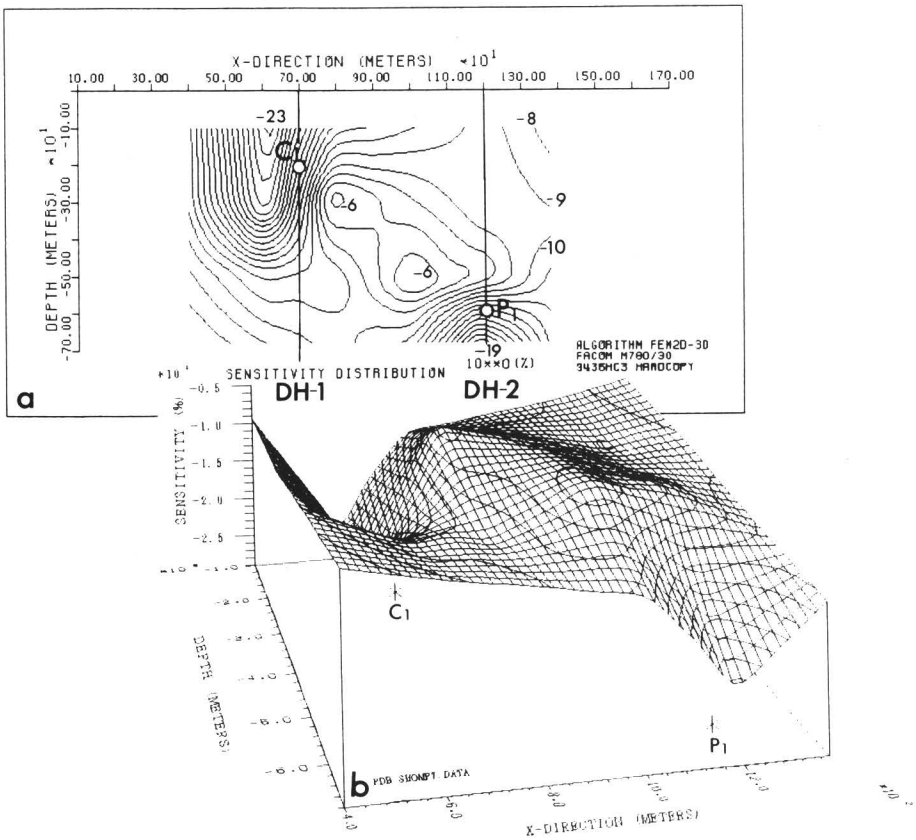

Fig. 3. An example of sensitivity distribution for C(subsurface) P(subsurface) cross-hole electrode array.
(a) : Two-dimensional contour section, (b) : Three-dimensional perspective view of section.

2) ρ_{aN}, the apparent resistivity (ohm-m) of the background.

3) $S_k=(\rho_{ak}-\rho_{aN})/\rho_{aN}\cdot 100$, the sensitivity (%) of the electrode array configuration, expressed in the center of the target inhomogeneity.

Figure 3 shows an example of the sensitivity distribution obtained by the FEM 2D-3D algorithm for C(subsurface) P(subsurface) pole-pole cross-hole solid electrode array system. The current electrode C_1 is located at the depth of 200 m in the borehole DH-1, and the potential electrode P_1 at the depth of 600 m in the borehole DH-2. The spacing of the boreholes is 500 m and the depths are 600 m. The xz-section size of the target inhomogeneity model is 2 * 2 units (1 unit : 100 m) as shown in Figure 2. The target model moves every two units in

the x and z–directions for this solid array configuration. Figure 3 a shows the two–dimensional contour plot of the percentage sensitivity distribution. Also, Figure 3 b shows the three–dimensional perspective plot of its sensitivity distribution on the xz–section. By the definition, the sensitivities in the cases of $S_k \leqq 0$ for the relation of $\rho_k \leqq \rho_N$ between the target resistivity ρ_k and the background resistivity ρ_N are called the normal sensitivities. Those in the case of $S_k \geqq 0$ for the same resistivity relation are called the reverse sensitivities, respectively. The high normal sensitivity peak whose value is about -23% is produced at the left side of the current electrode C_1. The high normal sensitivity peak of about -19% is produced at the right side of the electrode P_1. The

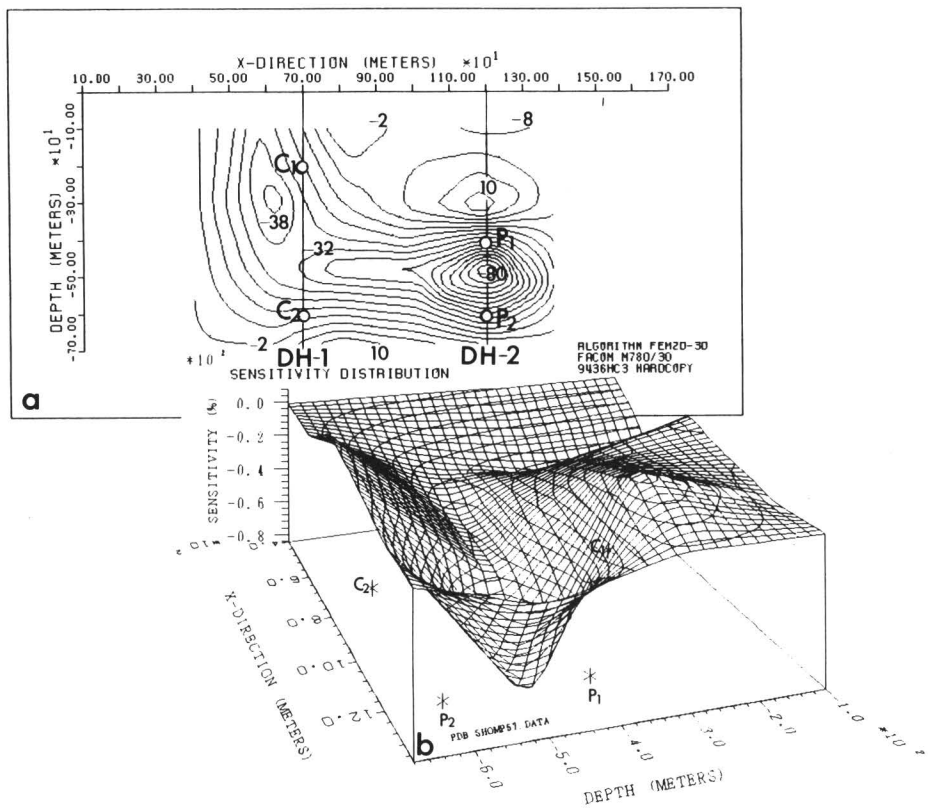

Fig. 4. An example of sensitivity distribution of CC(subsurface) PP(subsurface) cross-hole electrode array.
(a) : Two-dimensional contour section, (b) : Three-dimensional perspective view of section.

low normal sensitivity zone of about $-6\,\%$ is produced between C_1 and P_1. This zone is produced by the effects of the reverse sensitivity characteristics. This pattern shows the typical characteristics of the pole–pole array system.

Figure 4 shows an example of the sensitivity distributions for the *CC* (subsurface) *PP* (subsurface) dipole–dipole cross–hole solid electrode array system. The current electrodes C_1 and C_2 are located at the depths of 200 m and 400 m in the borehole DH–1, and the potential electrodes P_1 and P_2 at the depths of 400 m and 600 m in the borehole DH–2. Figure 4 a shows the two–dimensional contour plot of the percentage sensitivity distribution. Also, Figure 4 b shows the three–dimentional perspective plot of its sensitivity distribution on the *xz*–section.

The high normal sensitivity peak whose value is about $-80\,\%$ is produced between the potential electrodes P_1 and P_2. The high normal sensitivity peak of about $-38\,\%$ is produced in the normal sensitivity zones at the left side of the electrode C_1. The reverse sensitivities of about $10\,\%$ are produced above the electrode P_1 and at the right side below the electrode P_2. The high normal sensitivity belt is produced between the C_1C_2 and P_1P_2. This sensitive pattern shows the typical characteristics of the dipole–dipole electrode array system.

At the stage of this sensitivity distribution modelings, it can be suggested that the four electrode system such as the dipole–dipole array is more sensitive than the two electrode pole–pole system to the response due to target inhomogeneities. As the result of the various sensitivity distribution modelings, it is not premature to conclude that the designing effective solid electrode–probing arrays will be a most important element.

3. Computerized section procedure using sensitivity distribution technique in solid array electrical prospecting

In the geoelectrical applications, we measure the potential distributions along borehole or tunnel and the ground surface resulting from the current sources located at various places in each borehole or tunnel and the surface. From these data, a computerized electrical resistivity section (tomograph) can be constructed by the use of the resistivity inversion technique. The electrical tomograph image reconstruction technique has become an attractive and powerful tool for geophysicists.

For surface geoelectrical data, Tripp et al. (1984) have already used a tomography technique as reported in the paper, Geophysics, vol. 49, no. 10.[33] In contrast to the surface electrode array system, the hole–to–surface and cross–hole

systems can sometimes be closer to the target inhomogeneity, and therefore have a higher sensitivity in the region of interest. Daily and Yorkey (1988) at Lawrence Livermore National Laboratory have presented the applications in the resistivity tomography[41] for the case of a two-layered structure having a conductive body. Their reconstructed values have errors as much as 26%. Their evaluation was accomplished in the case of *CC*(borehole) *PP*(another borehole) cross-hole array system.

To solve the inverse problem in tomographic analysis, various reconstruction algorithms are proposed by several investigators. The problems are the design of sensitive electrode configurations and array combination patterns, setting of effective reasonal initial models, processing by shorter CPU, analysis of more complicated structures, interpretation of noise data, diagnosis of model optimization using Akaike's Bayesian information criterion etc., and field applications. In this investigation, an evaluation is made of solid electrode array effects in the computerized section construction by the sensitivity distribution technique.

Figure 5 shows a way of doing the solid array electrical measurements between a vertical borehole and the horizontal surface. Figure 5 a illustrates the *CC*(borehole DH-1) *PP*(surface) electrode combination pattern, in which the

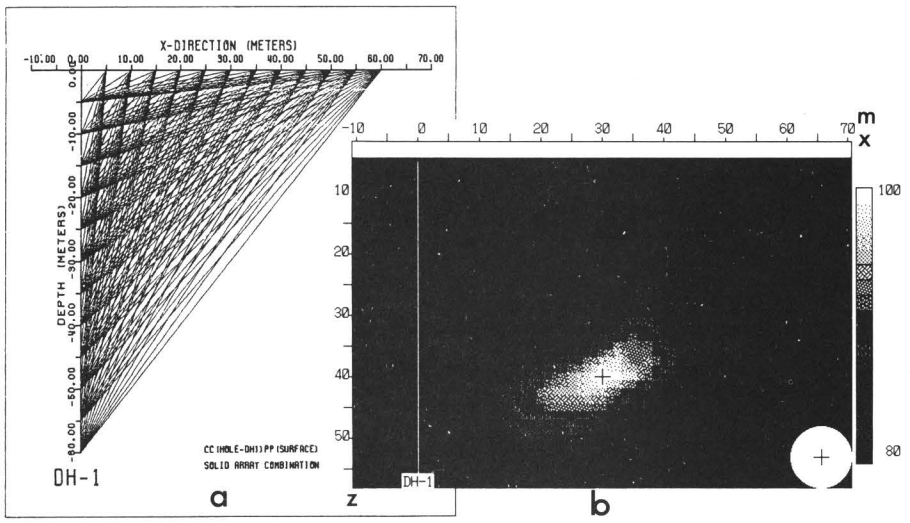

Fig. 5. An example of resistivity computerized section for CC (subsurface) PP(surface) solid array. (a) : CC(borehole DH-1) PP(surface) hole-to-surface array combination pattern, (b) : Resistivity computerized section obtained by the construction procedure.

current electrodes C_1 and C_2 are driven in the same borehole from the depth of 5 m to 60 m and the potential electrodes P_1 and P_2 on the surface at 5 m from the top of the borehole to 60 m in the x-direction.

There are 12 electrode positions (10 m spacing) along borehole DH-1 and 12 electrode positions (also 10 m spacing) on the surface. With these 24 electrodes, one can obtain 100 unique apparent resistivity data using the *CC*(subsurface) *PP* (surface) dipole-dipole solid array. Also, one can provide 100 unique sensitivity distributions for the *CC*(subsurface) *PP*(surface) electrode arrangements. Consequently, each apparent resistivity can be transformed to the probability distribution for the *CC*(borehole DH-1) *PP*(surface) solid array system in the region of geophysical interest. Finally, the initial computerized section shown in Figure 5 b can be obtained. In this example, the radius of the spherical conductive target inhomogeneity is 5 m, and the location of its center is 40 m in depth. The probability zone of 100% calculated by the sensitivity distribution technique means the perfect presence of the target inhomogeneity at that area.

4. Evaluation of solid array effects in electrical computerized section procedure

4.1 Solid array configuration effects

Figure 6 a shows an example of the resistivity computerized section for the *C*(subsurface) *P*(surface) pole-pole hole-to-surface electrode array system. The target inhomogeneity model is a perfect conductive sphere in the background medium of resistivity $\rho_0 = 100$ ohm-m. It exists at the depth z of 40 m and the distance x from the top of the borehole DH-1 which is 30 m. The position of its center is indicated by the cross symbol '+' in Figure 6 a. Also, the radius of the target sphere is 5 meters. Its size in the figure is indicated by the white circle at the right corner of Figure 6 a. This computerized section is reconstructed by using 144 data which consist of 12 subsurface (borehole DH-1) current electrodes and 12 surface potential electrodes, the same as shown in Figure 5 a. The high probability value of over 90% is produced at the rather wide area including the center of the target sphere. Figure 6 b shows the computerized resistivity section for the *C*(subsurface) *PP*(surface) pole-dipole hole-to-surface electrode array system in the case of the same target inhomogeneity. It is reconstructed with 120 data which consist of 12 subsurface (borehole DH-1) current electrodes and 10 surface potential *PP* electrodes, the same as shown in Figure 5 a. As shown in Figures 6 a and 6 b, the high probabilities of over 90% are produced at the areas including the center of the target body and its surrounding back-

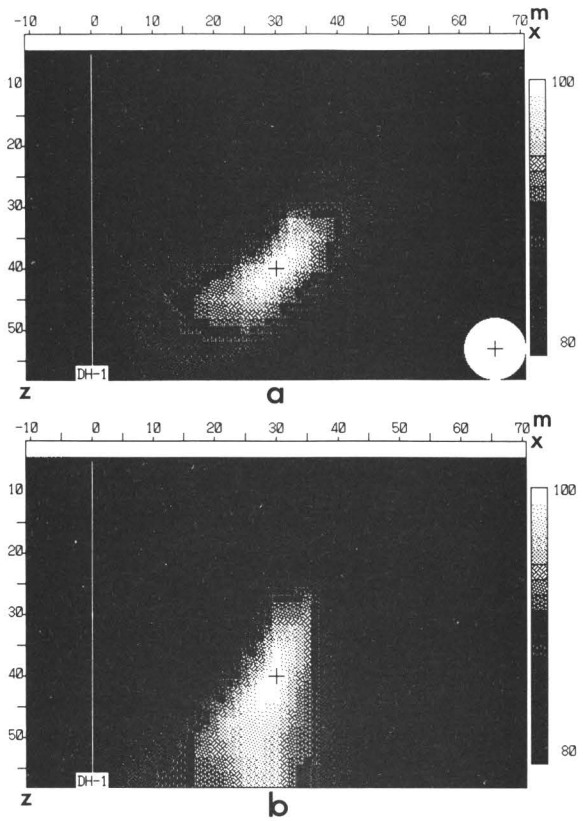

Fig. 6. Evaluation of solid array configuration effects in resistivity computerized sections obtained by the construction procedures. (a) : Section for C (borehole DH-1) P (surface) hole-to-surface array combination, (b) : Section for C (borehole DH-1) PP (surface) hole-to-surface array combination.

ground.

The result of the computerized section for *CC*(subsurface) *PP*(surface) has been already illustrated in Figure 5 b. By comparison with the case of *CC* (borehole DH-1) *PP*(surface), the section of *C*(borehole DH-1) *P*(surface) shown in Figure 6 a indicates less focussed anomalies over the spherical conductive target inhomogeneity. Also, the section of *C*(borehole DH-1) *PP*(surface) shown in Figure 6 b has more undetectable anomalies than the result of the *CC* (subsurface) *PP*(surface) dipole-dipole array system shown in Figure 5 b. These

observations have important consequences when various subsurface solid arrays are discussed for a more sensitive detection of subsurface structures or more effective monitoring of the changes in the resistivity of subsurface spaces. It should also be noted from Figures 5 b, 6 a and 6 b that the best focussed anomalies are obtained when the *CC*(subsurface) *PP*(surface) dipole-dipole array configuration is applied to detect the target of interest.

4.2 Solid array spacing and line effects

From a practical point of view, it is also important to note the solid array spacing and line effects in order to design effective arrays under subsurface measuring conditions in the fields.

Figures 7 a and 7 b show the examples of *CC*(borehole DH-1) *PP*(surface) solid electrode array combination patterns. Figure 7 a illustrates a hole-to-surface electrode array combination in which the current electrodes C_1 and C_2 (10 m spacing) are driven in the same borehole with 12 electrode positions from the depth of 5 m to 60 m and the potential electrodes P_1 and P_2 (30 m spacing) on the surface with 12 electrode positions from the horizontal distance of 5 m to 80 m, and by which 100 unique apparent resistivity data are obtained. Next, Figure 7 b illustrates a hole-to-surface electrode combination in which the current electrodes C_1 and C_2 (10 m spacing) are driven in the same borehole with 8 electrode positions from the depth of 45 m to 80 m and the potential electrodes P_1 and P_2 (30 m spacing) on the surface with 12 electrode positions from the horizontal distance of 5 m to 80 m, by which 60 unique apparent resistivity data are obtained.

Figure 8 a shows an example of the resistivity computerized section for the *CC*(borehole DH-1) *PP*(surface) solid electrode array system as shown in Figure 7 a. The target inhomogeneity model is the same perfect conductive sphere in the medium of resistivity $\rho_0 = 100$ ohm-m as already shown in Figure 5 b. The position of its center is at the depth z of 40 m, and the distance x from the borehole DH-1 is 30 m. This is indicated by the cross symbol '+' in Figure 8 a. Also, the radius of the target body is 5 meters. Its size is indicated by the white circle at the right corner in Figure 8 a. This computerized section is reconstructed with 100 data, which consist of 10 subsurface (borehole DH-1) current electrode pairs C_1C_2 (10 m spacing) and 10 surface potential electrode pairs P_1P_2 (30 m spacing) as shown in Figure 7 a. The high probability of over 90 % is produced in the similarly inclined and more focussed area than the case of Figure 5 b, which image is reconstructed by the surface potential electrode pairs P_1P_2 (10 m spacing). This change clearly shows the spacing effect. To

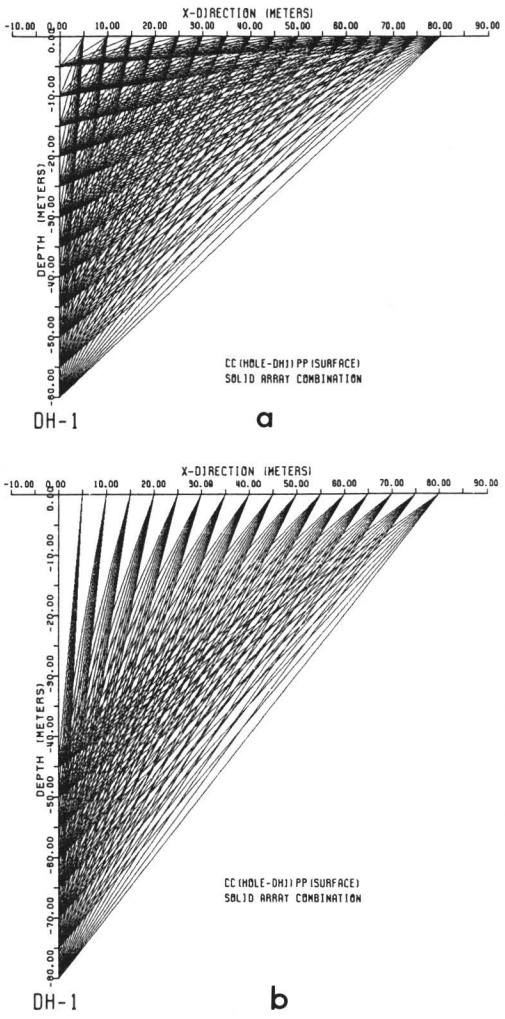

Fig. 7. Combination patterns of CC(subsurface) PP (surface) hole-to-surface array configurations. (a) : CC (driven in the borehole DH-1 from the depth of 5 m to 60 m with a spacing of 10 m), PP (driven on the surface from the distance of 5 m to 80 m in the x-direction with a spacing of 30 m) solid array system, (b) : CC (driven in the borehole DH-1 from the depth of 45 m to 80 m with a spacing of 10 m), PP (driven on the surface from the distance of 5 m to 80 m with a spacing of 30 m) solid array system.

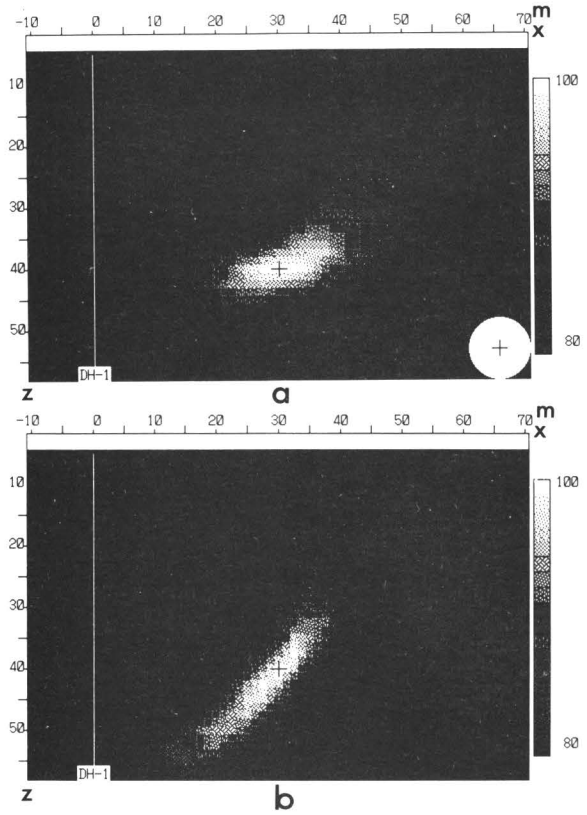

Fig. 8. Evaluation of solid array spacing and line effects in resistivity computerized sections obtained by the construction procedures.
(a) : Section in the case of Fig. 7a,
(b) : Section in the case of Fig. 7b.

select the proper spacings of electrodes produces good results in not only the measurements of potential differences but also the resistivity computerized section construction procedure. Figure 8 b shows the resistivity computerized section for the data obtained by the *CC*(6 electrode pairs, 10 m spacing, from the depth of 45 m to 80 m in the borehole DH- 1) *PP*(10 electrode pairs, 30 m spacing, from the distance of 5 m to 80 m on the surface) solid array system as shown in Figure 7 b. The high probabilities of over 90 % are produced in the slightly inclined and rather more focussed area, including the center of the target body and its surrounding background, than the case of Figure 8 a. The line effect may appear because of the deeper C_1C_2 electrode combination which covers the

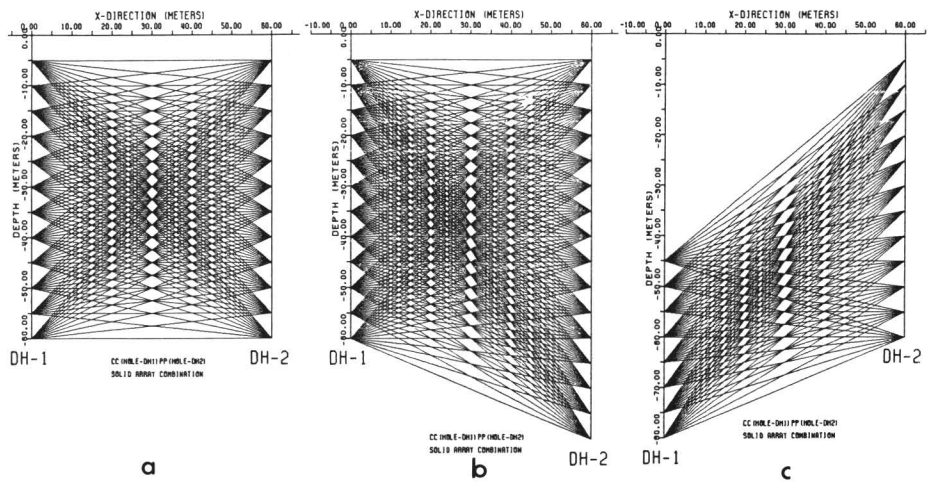

Fig. 9. Combination patterns of CC (subsurface) PP (subsuface) cross-hole array configurations. (a) : CC(driven in the borehole DH-1 from the depth of 5 m to 60 m with a spacing of 10 m), PP(driven in the borehole DH-2 from the depth of 5 m to 60 m with a spacing of 10 m), (b) : CC(driven in the borehole DH-1 from the depth of 5 m to 60 m with a spacing of 10 m), PP(driven in the borehole DH-2 from the depth of 5 m to 80 m with a spacing of 10 m), (c) : CC(driven in the borehole DH-1 from the depth of 45 m to 80 m with a spacing of 10 m) PP(driven in the borehole DH-2 from the depth of 5 m to 60 m with a spacing of 10 m).

area of the target inhomogeneity with a higher density than the case of Figure 8 a.

Figures 9 a, 9 b and 9 c are the examples of *CC*(borehole DH-1) *PP*(borehole DH-2) cross-hole array systems for the examination of the line effects. Figure 9 a illustrates the *CC*(subsurface) *PP*(subsurface) array combination pattern consisting of 10 subsurface (borehole DH-1) current electrode pairs C_1C_2 (10 m spacing) and 10 subsurface (borehole DH-2) potential electrode pairs P_1P_2 (10 m spacing), which provide 100 data. Figure 9 b illustrates the combination pattern consisting of 10 subsurface (borehole DH-1) current electrode pairs C_1C_2 (10 m spacing) and 14 subsurface (borehole DH-2) potential electrode pairs P_1P_2 (10 m spacing) from the depth of 5 m to 80 m, which provide 140 data. Figure 9 c illustrates the combination pattern consisting of 6 subsurface (borehole DH-1) current electrode pairs C_1C_2 (10 m spacing) from the depth of 45 m to 80 m and 10 subsurface (borehole DH-2) potential electrode pairs P_1P_2 (10 m spacing), which provide 60 data.

Figures 10 a, 10 b and 10 c show the resistivity computerized sections in the

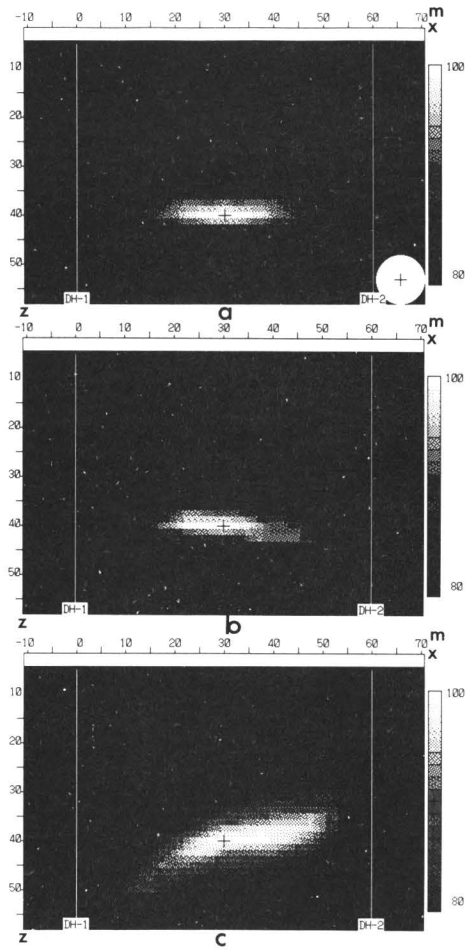

Fig. 10. Evaluation of solid array spacing and line effects in resistivity computerized sections obtained by the construction procedures.
(a) : Section in the case of Fig. 9a,
(b) : Section in the case of Fig. 9b,
(c) : Section in the case of Fig. 9c.

cases of Figures 9 a, 9 b and 9 c, respectively. Comparing these three figures, the longer line case in the borehole DH-2 shown in Figure 10 b indicates the inclined focussed area. The shorter line case in the borehole DH-1 shown in Figure 10 c indicates the more inclined and less focussed area, but with rather good results, respectively.

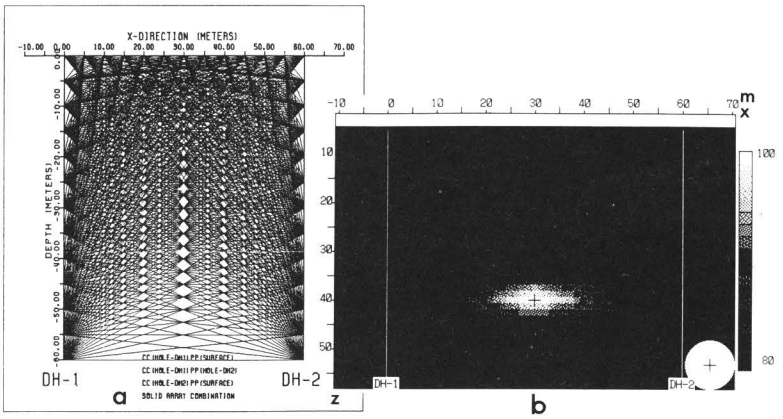

Fig. 11. Resistivity computerized section for a combination of CC(borehole DH-1) PP (surface), CC(borehole DH-2) PP(borehole DH-2) solid array configurations.
(a) : Illustration of electrode array combination pattern,
(b) : Resistivity computerized section obtained by the construction procedure.

As a result of the examinations, it may be necessary to take into account the solid array line effects in order to select the effective and reasonable array combinations, which extract and enhance the responses due to the target inhomogeneities in the resistivity computerized sections.

4.3 Solid array combination effects

From a more practical point of view, it is also important to note the solid array combination or composition effects in designing solid array patterns for the good extraction and enhancement of responses due to the target inhomogeneities under the various complicated measuring conditions.

Figure 11 a shows an example of *CC*(borehole DH-1) *PP*(surface), *CC* (borehole DH-2) *PP*(surface) and *CC*(borehole DH-1) *PP*(borehole DH-2) solid array combination, in which the current *CC*(subsurface) electrode pairs (10 m spacing) are driven in the borehole DH-1 or DH-2 from the depth of 5 m to 60 m, respectively, and the potential *PP*(surface) electrode pairs (10 m spacing) in the x-direction. Figure 11 b indicates the resistivity computerized section for the dipole-dipole typed cross-hole and hole-to-surface electrode array combination as shown in Figure 11 a, in which the array combination effect is investigated. The target inhomogeneity model is the same as the examples of Figure 5 b. This target exists in the depth z of 40 m and the distance x of 30 m from the borehole DH-1. The center is indicated by the cross symbol '+' in

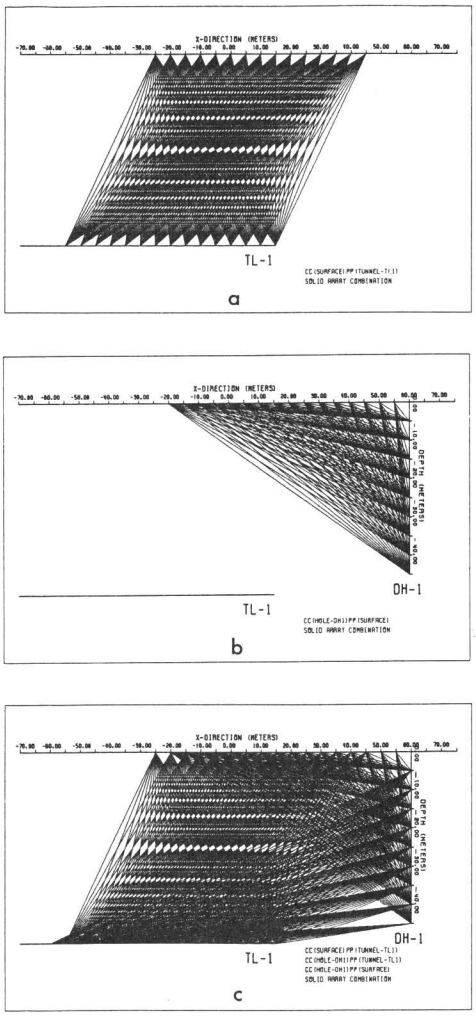

Fig. 12. Combination pattern of solid array configurations using tunnel, borehole and ground surface. (a) : CC(driven on the surface from the distance of -25 m to 45 m with a spacing of 5 m), PP(driven in the tunnel TL-1 from the distance of -55 m to 15 m with a spacing of 25 m), (b) : CC(driven in the borehole DH-1 from the depth of 5 m to 45 m with a spacing of 10 m), PP(driven on the surface from the distance of -20 m to 55 m with a spacing of 10 m), (c) : (a), (b) and CC(driven in the borehole DH-1 from the depth of 5 m to 45 m with a spacing of 10 m), PP(driven in the tunnel TL-1 from the distance of -60 m to 15 m with a spacing of 30 m) electrode array combinations.

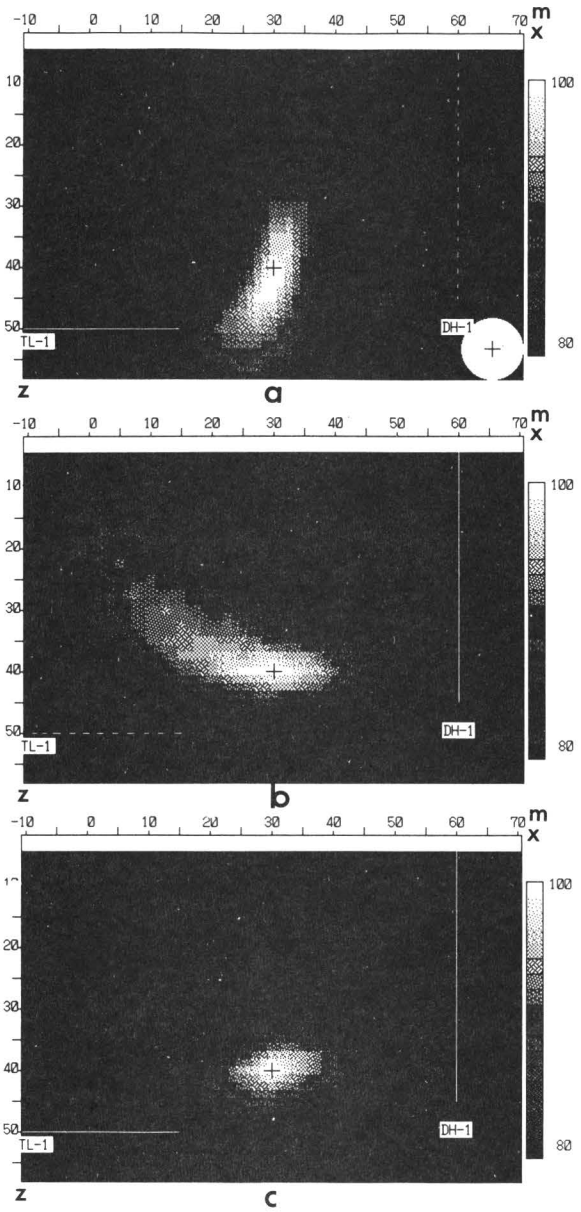

Fig. 13. Evaluation of solid array combination effects in resistivity computerized sections obtained by the construction procedures.
(a) : Section in the case of Fig. 12a,
(b) : Section in the case of Fig. 12b,
(c) : Section in the case of Fig. 12c.

Figure 11 b. Also, the radius of the target body is 5 meters, which is indicated by the white circle under the right corner in Figure 11 b.

This computerized section is reconstructed with 300 data, which consist of 12 subsurface (borehole DH-1) electrodes, 12 subsurface (borehole DH-2) electrodes and 12 surface electrodes combination as shown in Figure 11 a. The high probability of over 90% is produced in the more sucessfully focussed area including the center of the target sphere.

Figures 12 a, 12 b and 12 c show three examples of the *CC*(surface) *PP*(tunnel TL-1), *CC*(borehole DH-1) *PP*(surface) and the combination of 12 a, 12 b and *CC*(borehole DH-1) *PP*(tunnel TL-1) systems. In the surface-to-tunnel array combination pattern as shown in Figure 12 a, the electrodes C_1 and C_2 (25 m spacing) are driven in the tunnel TL-1 from the distance of -55 m to 15 m. The electrodes P_1 and P_2 (5 m spacing) on the surface from the distance of -25 m to 45 m are in the x-direction. Next, in the borehole-to-surface array combination pattern as shown in Figure 12 b, the electrodes C_1 and C_2 (10 m spacing) are driven in the borehole DH-1 from the depth of 5 m to 45 m. The electrodes P_1 and P_2 (10 m spacing) on the surface from the distance of -20 m to 55 m are in the x-direction. Also, in the combined solid array system shown in Figure 12 c, including the borehole-to-tunnel array combination pattern, the electrodes C_1 and C_2 (10 m spacing) driven in the borehole DH-1 from the depth of 5 m to 45 m, and the electrodes P_1 and P_2 (10 m spacing) driven in the tunnel TL-1 from the distance of -60 m to 15 m are added. The conductive target inhomogeneity with the resistivity $\rho_k = 0$ ohm-m exists in the medium of resistivity $\rho_0 = 100$ ohm-m at the depth z of 40 m and the distance x of 30 m.

Figures 13 a, 13 b and 13 c show the resistivity computerized sections for the *CC*(surface) *PP*(tunnel TL-1), the *CC*(borehole DH-1) *PP*(surface) and the combination of 12 a, 12 b and the *CC*(borehole DH-1) *PP*(tunnel TL-1) arrays. The sections are reconstructed with 140, 98 and 308 data, respectively. The high probabilities of over 90% in Figures 13 a, 13 b and 13 c are produced in the area including the center of the target body. Compared with each other, Figure 13 b indicates less focussed anomalies for the spherical conductive target inhomogeneity than Figures 13 a or 13 c. It may be reflected by the distance from the borehole DH-1 to the tunnel TL-1 and the small 70 data. Figure 13 a indicates that the surface-to-tunnel solid arrays may be able to detect the subsurface structures ahead of the tunnel under construction and to monitor the resistivity changes in its hydrogeological environments, in some degree, without other arrays. It should also be noted from the results shown in Figures 13 a, 13 b and 13 c that indeed, the best focussed anomalies occur when the combina-

tion of *CC*(surface) *PP*(tunnel TL-1), *CC*(surface) *PP*(borehole DH-1) and *CC* (borehole DH-1) *PP*(tunnel TL-1) solid array configurations is applied to detect the zone of interest.

Generally, in the complex resistivity environments, it is very important how to reduce the various non-target inhomogeneity effects for the extraction and enhancement of the response (signal) due to the target. Hence, the effective solid electrode array combinations should be carefully selected among the sensitive arrays under the various conditions by using the modelings, such as the sensitivity distribution technique.

5. Conclusions

The effects of the solid electrode array cofigurations and of the array combination patterns in the resistivity computerized section comstruction procedure have been evaluated by using the FEM 2D-3D algorithm and the sensitivity distribution technique. A future work is to design effective solid electrode array configurations in the field applications under the various exploration environments, such as cross-hole(tunnel) and hole(tunnel)-to-surface conditions. The results drawn from these model studies should provide a useful suggestion as an aid to design the effective solid array configurations and combinations. Some results in this investigation are as follows:

1) The evaluation of solid array effects in resistivity computerized section was performed by the sensitivity distribution technique.

2) In the evaluation of solid array configuration effects, the resistivity computerized sections of *C*(subsurface) *P*(surface), *C*(subsurface) *PP*(surface) and *CC*(subsurface) *PP*(surface) hole-to-surface electrode arrays have been constructed. From the results, it is recognized that the best focussed anomalies are reconstructed over the conductive spherical target inhomogeneity when the dipole-dipole array configuration is applied to detect the target of interest.

3) In the evaluation of solid array spacing and line effects, the computerized sections of *CC*(subsurface) *PP*(surface) hole-to-surface arrays with spacings of 10 m and 30 m and *CC*(subsurface) *PP*(subsurface) cross-hole arrays with lines 60 m and 80 m have been investigated. The focussed areas appear in various types by the effects of the array spacings and lines.

4) In the evaluation of solid array combination effects, the computerized sections of *CC*(subsurface and surface) *PP*(subsurface and surface) using

the combinations of boreholes DH-1, DH-2 and surface, and also tunnel TL-1, borehole DH-1 and surface have been examined. The combined solid array information provides more focussed anomalies over the target of interest.

Recently, the growing use of computer simulation increases a demand for the investigations and the development of interpretation methods. Numerical modeling including the visualization technique and the use of subsurface electrodes have been new elements of the most important recent developments in electrical survey methods. Electrical methods using subsurface electrodes have become increasingly more useful exloration tools for detecting deep or hidden mineral deposits, energy or ground-water resources and geological fracture zones, and also for monitoring groundwater contamination, nuclear waste repository and various changes of earth structures.

In the future, the effectiveness of the electrical technique depends upon its ability to interpret the large 3-D data of high density obtained under more complex structure environments and more difficult measuring conditions.

Acknowledgement

The author is very grateful to Professor Koichi Sassa, Department of Mineral Science and Technology, Faculty of Engineering, Kyoto University, for his valuable comments and suggestions for this manuscript.

The numerical simulation and visualization were performed by the Fujitsu computer FACOM M 780 system at the Data Processing Center of Kyoto University. This work was supported by the Grant-in-Aid for Scientific Research (62850115) of the Ministry of Education and Culture in Japan.

References

1) T. Sugano, Applications of electrical prospecting methods to mineral exploration and evaluation, presented at Ann. Mtg., MMIJ, A-3, pp. 7-11, 1982.

2) SEGJ, Electrical and electromagnetic prospecting: Methods and principles, Illustrations of Geophysical Prospecting, pp. 53-62/pp. 192-201, 1989.

3) T. Sugano, Electrical resistivity pilot survey using borehole solid electrode arrays, Seikan Tunnel Geophysical Exploration Committee, Report 49-3 (in Japanese), pp. 22-23, 1974.

4) T. Sugano and K. Sassa, Cross-hole and hole-to-surface resistivity modeling, Geophysical Exploration (Butsuri-tansa), vol. 41, no. 1, pp. 1-17, 1988.

5) T. Sugano and K. Sassa, Normalization procedure of non-target inhomogeneities for

resistivity interpretation, presented at Mtg. of Nondestructive Inspection, NDI-no. 3881, pp. 43 - 50, 1987.

6) T. Sugano and K. Sassa, Expression procedure in an evaluation of resistivity interpretation process, Geophysical Exploration (Butsuri-tansa), vol. 41, no. 2 ,pp. 116 - 132, 1988.

7) J. J. Daniels and A. V. Dyck, Borehole resistivity and electromagnetic methods applied to mineral exploration, IEEE Trans. on Geosci. and Remote Sensing, vol. GE- 22, pp. 80 - 87, 1984.

8) J. J. Daniels, Hole-to-surface resistivity measurements, Geophysics, vol. 48, pp. 87 - 97, 1983.

9) J. J. Daniels, Three-dimensional resistivity and induced-polarization modeling using buried electrodes, Geophysics, vol. 42, pp. 1006 - 1019, 1977.

10) T. E. Owen, Detection and mapping of tunnels and caves, Developments in Geophysical Exploration Methods, 5, pp. 161 - 258, 1983.

11) J. O. Parra and T. E. Owen, Model studies of electrical leak detection surveys in geomembrance-lined impoundments, Geophysics, vol. 53, pp. 1453 - 1458, 1988.

12) R. J. Lytle, Resistivity and induced-polarization probing in the vicinity of a spherical anomaly, IEEE Trans. Geosci. Remote Sensing, vol. GE- 22, pp. 493 - 499, 1982.

13) R. J. Lytle and J. M. Hanson, Electrode conflguration influence on resistivity measurements about a spherical anomaly, Geophysics, vol. 48, pp. 1113 - 1119, 1983.

14) T. Sugano, A fundamentary study on resistivity interpretation, Msc. thesis, Kyoto Univ., 1968.

15) MMIJ, A study on sensitivity distribution of electrode configuration, Physical Properties of Minerals and Rocks and Geophysical Data Processing (in Japanese), pp. 168 - 174, 1974.

16) SEGJ, Sensitivity distribution, Encyclopedic Dictionary of Exploration Geophysics, pp. 63 - 64, 1978.

17) R. D. Baker, Signal contribution sections and their use in resistivity studies, Geophysical Journal of the Royal Astromical Society, vol. 59, pp. 123 - 129, 1979.

18) E. Gomez-Trevino, A simple sensitivity analysis of time-domain and frequency-domain electromagnetic measurements, Geophysics, vol. 52, pp. 1418 - 1423, 1987.

19) R. Bazinet and P. Berube, Lateral Pole-pole : A "new" array for increasing induced-polarization survey perfomance, presented at the 58 th Ann. Internat. Mag., SEG, pp. 246 - 248, 1988.

20) T. Sugano, K. Sassa, Evaluation of solid electrode array offects as an aid to computerized section procedure in electrical prospecting method, Journal of the Society of Materials Science (Zairyo), vol. 39, to be published, 1990.

21) L. Alfano, Geoelectric prospecting with underground electrodes, Geophysical Prospecting, vol. 10, pp. 290 - 303, 1962.

22) R. H. Merkel and S. S. Alexander, Resistivity analysis for models of a sphere in a half -space with buried current source, Geophysical Prospecting, vol. 19, pp. 640 - 651, 1971.

23) J. H. Coggon, Electromagnetic and electrical modeling by the finite element method, Geophysics, vol. 36, pp. 132 - 155, 1971.

24) L. Rijo, Modeling of electric and electromagnetic data, Ph. D. dissertation, Univ. of

Utah, 1977.
25) D. F. Pridmore, Three dimensional modeling of electric and electromagnetic data using the finite element method, Ph. D. dissertation, Univ. of Utah, pp. 144 - 185, 1978.
26) H. T. Holcombe and G. R. Jiracek, Three-dimensional terrain corrections in resistivity surveys, Geophysics, vol. 49, pp. 439 - 452, 1984.
27) A. Jämtlid, K. A. Magnussen, O. Olsson and L. Stenberg, Electrical borehole measurements for the mapping of fracture zones in crystalline rocks, Geoexploration, vol. 22, pp. 203 - 216, 1984.
28) F. W. Yang and S. H. Ward, On sensitivity of surface-to-borehole resistivity measurements to the depth to center of a three-dimensional spheroid, Geophysics, vol. 50, pp. 1173 - 1178, 1985.
29) J. X. Zhao, L. Rijo and S. H. Ward, Effects of geologic noise on cross-borehole electrical surveys, Geophysics, vol. 51, pp. 1978 - 1991, 1986.
30) C. W. Beasley and S. H. Ward, Three-dimensional mise-à-la-masse modeling applied to mapping fracture zones, Geophysics, vol. 51, pp. 98 - 113, 1986.
31) M. L. Oristaglio and M. H. Worthington, Inversion of subsurface and borehole electromagnetic data for two-dimensional electrical conductivity models, Geophysical Prospecting, vol. 28, pp. 633 - 657, 1980.
32) M. H. Worthington, An introduction to geophysical tomography, First Break, European Association of Exploration Geophysicists, vol. 2, pp. 20 - 26, 1984.
33) A. C. Tripp, G. W. Hohmann, and C. M. Swift, Jr., Two-dimensional resistivity inversion, Geophysics, vol. 49, pp. 1708 - 1717, 1984.
34) K. A. Dines and R. J. Lytle, Analysis of electrical conductivity imaging, Geophysics, vol. 46, pp. 1025 - 1036, 1981.
35) T. Murai and Y. Kagawa, Electrical impedance computed tomography based on a finite element method, IEEE Trans. on Biomed. Eng., vol. BME-32, pp. 177 - 184, 1985.
36) D. Isaacson, Distinguishability of conductivities by electric current computed tomography, IEEE Trans. on Medical Imaging, vol. MI-5, pp. 91 - 95, 1986.
37) T. J. Yorkey, J. G. Webster and W. J. Tompkins, Comparing reconstruction algorithms for electrical impedance tomography, IEEE Trans. on Biomed. Eng., vol. BME-34, pp. 843 - 852, 1987.
38) T. Sugano and K. Sassa, Problems of electrical prospecting: Evaluation of extraction and enhancement of response due to target inhomogeneities in cross-hole and hole-to-surface due to target inhomogeneities in cross-hole and hole-to-surface array methods, Geotomography Applications to Rock Engineering, presented at Ann. Mtg., MMIJ, E-3, pp. 9 - 12, 1989.
39) T. Sugano and K. Sassa, Development of elements as an aid to solid resistivity array prospecting method using cross-hole and hole-to-surface electrode configuration, Suiyokwai-shi (in Japanese), vol. 21, no. 2, pp. 115 - 125, 1989.
40) T. Sugano and K. Sassa, Pseudosections for electrical solid array resistivity interpretation, Geophysical Exploration, vol. 42, no. 4, pp. 253 - 270, 1989.
41) W. Daily and T. J. Yorkey, Evaluation of cross-hole resistivity tomography, presented at SEG Mtg., Houston, pp. 201 - 203, 1988.
42) C. W. Beasley and S. H. Ward, Cross-borehole resistivity inversion, presented at SEG

Mtg., Houston, pp. 198 - 200, 1988.

43) D. Le Masne and C. Poirmeur, Three-dimensional model results for an electrical hole-to-surface method: Application to the interpretation of a field survey, Geophysics, vol. 53, pp. 85 - 103, 1988.

44) T. Asch and H. F. Morrison, Mapping and monitoring electrical resistivity with surface and subsurface electrode arrays, Geophysics, vol. 54, pp. 235 - 244, 1989.

45) T. Lowry, M. B. Allen and P. N. Shive, Singularity removal: A refinement of resistivity modeling techniques, Geophysics, vol. 54, pp. 766 - 774, 1989.

46) G. J. Palacky, Tutorial: Research, applications and publications in electrical and electromagnetic methods, Geophysical Prospecting, vol. 31, pp. 861 - 872, 1983.

47) G. J. Palacky, Resistivity characteristics of geologic targets, Investigations in Geophysics no. 3, Society of Exploration Geophysicists, pp. 52 - 129, 1987.

48) T. Sugano, Extraction and enhancement of signal due to subsurface target inhomogeneities by using electrical prospecting method, Geological Data Processing, 14, in printing, 1989.

49) T. Sugano and K. Sassa, Evaluation of extraction and enhancement of response due to target inhomogeneities for resistivity interpretation, Memoirs of Faculty of Eng. Kyoto Univ., vol. 51, no. 1, pp. 10 - 38, 1989.

50) H. Akaike, A new look at the statistical model identification, IEEE Trans., vol. AC- 19, pp. 716 - 723, 1974.

51) J. V. Beck and K. J. Arnold, Parameter estimation in engineering and science, John Wiley & Sons.

52) J. M. Ortega and W. C. Rheinbolt, Interactive solutions of nonlinear equations in several variables, Academic Press, New York, 1970.

53) O. Z. Zienkiewicz, The finite element method in engineering science, Mcgraw-Hill, New York, 1971.